ЖЭТФ, 2007, том 131, вып. 2, стр. 259–274

ELECTRON SPECTRUM IN HIGH-TEMPERATURE CUPRATE SUPERCONDUCTORS

N. M. Plakida [*a,b], ***V. S. Oudovenko*** [a,c]

[a] *Joint Institute for Nuclear Research, Dubna, Russia*

[b] *Max-Planck-Institut für Physik Komplexer Systeme, Dresden, Germany*

[c] *Rutgers University, New Jersey, USA*

Received 7 July 2006

A microscopic theory for the electron spectrum of the CuO_2 plane within an effective p–d Hubbard model is proposed. The Dyson equation for the single-electron Green's function in terms of the Hubbard operators is derived and solved self-consistently for the self-energy evaluated in the noncrossing approximation. Electron scattering on spin fluctuations induced by the kinematic interaction is described by a dynamical spin susceptibility with a continuous spectrum. The doping and temperature dependence of electron dispersions, spectral functions, the Fermi surface, and the coupling constant λ are studied in the hole-doped case. At low doping, an arc-type Fermi surface and a pseudogap in the spectral function close to the Brillouin zone boundary are observed.

PACS: 74.20.Mn, 71.27.+a, 71.10.Fd, 74.72.-h

1. INTRODUCTION

Recent high-resolution angle-resolved photoemission spectroscopy (ARPES) studies revealed a complicated character of the electronic structure and quasiparticle (QP) spectra in copper oxide superconductors. In particular, a pseudogap in the electron spectrum and an arc-type Fermi surface (FS) at low hole concentrations were revealed, a substantial wave-vector and energy dependent renormalization of the Fermi velocity of QP ("kinks" in the dispersion) was observed (see, e.g., [1–3] and the references therein). As was originally pointed out by Anderson [4], strong electron correlations in cuprates play an essential role in explaining their normal and superconducting properties.

A conventional approach to describing strong electron correlations is based on the Hubbard model [5]. The model has some advantages in comparison with the t–J model, which can be derived from the Hubbard model in the limit of strong correlations. Namely, the Hubbard model allows studying a moderate correlation limit observed experimentally in cuprates and more consistently accounts for the two-subband character of the electron structure, in particular, a weight transfer between subbands with doping.

Various methods were proposed to study the electron structure within the Hubbard model. But an unbiased method based on numerical simulations for finite clusters (see, e.g., [6] for a review) does not allow studying subtle features of QP spectra due to poor energy and wave-vector resolutions in small-size clusters. In analytic calculations of spectra, mean-field-type approximations are often used (see [7, 8] for a review), which cannot reproduce the above-mentioned effects caused by the self-energy contributions. In the dynamical mean-field theory (DMFT) (see [9, 10] for a review), the self-energy is treated in the single-site approximation, which is also unable to describe wave-vector-dependent phenomena. To overcome this flaw of DMFT, various types of the dynamical cluster theory were developed (see [11, 12] for a review). In these methods, only a restricted wave-vector and energy resolutions can be achieved, depending on the size of the clusters, while the physical interpretation of the origin of an anomalous electronic structure in numerical methods is not straightforward.

To elucidate the pseudogap formation mechanism,

*E-mail: plakida@theor.jinr.ru

the scattering of charge carriers by short-range (static) antiferromagnetic (AF) spin fluctuations was considered in several analytic semi-phenomenological studies (see [2] for a review). More recently, with an additional momentum-dependent component of the self-energy originating from short-range AF (or charge) correlations included into the DMFT scheme, the spin-fluctuation scenario of the pseudogap formation [13] and the arc-type FS [14] were supported (see [15] for a review). At the same time, it is important to study the effects of the charge carrier scattering by the dynamical spin fluctuations, which are believed to be responsible for the kink phenomenon [3]. This can be done by considering the Dyson equation for the single-particle Green's function (GF) within the Hubbard model in the limit of strong correlations. For instance, calculation of the electron spectrum within the first-order perturbation theory for the self-energy has reproduced the quantum Monte Carlo results quite accurately [16], while application of the incremental cluster expansion for the self-energy has enabled observing a kink structure in the QP spectrum [17].

The aim of the present paper is to develop a microscopic theory for the electron spectrum in strongly correlated systems, such as cuprates, which consistently takes the effects of electron scattering by dynamical spin fluctuations into account. For this, we consider an effective Hubbard model reduced form the p–d model for the CuO_2 plane in cuprates. Applying the Mori-type projection technique for the thermodynamic GF [18] in terms of the Hubbard operators, we derive an exact Dyson equation, as was elaborated in our previous publications [19–21]. The Dyson equation with the self-energy evaluated in the noncrossing approximation (NCA) beyond the perturbation theory approach is then solved self-consistently.

This allows us to calculate the dispersion and spectral functions of single-particle excitations, the FS, and the electron occupation numbers. In particular, we study the hole-doped case at various hole concentrations. At low doping, the FS reveals an arc-type shape with a pseudogap in the $(\pi, 0)$ region of the Brillouin zone (BZ). A strong renormalization effects of the dispersion close to the Fermi energy ("kinks") are observed due to electron scattering by dynamical AF spin fluctuations induced by the kinematical interaction generic for the Hubbard operators. Electron occupation numbers show only a small drop at the Fermi energy. For high temperature or large hole concentrations, AF correlations become weak and a crossover to a Fermi-liquid-like behavior is observed.

In the next section, we briefly discuss the model and the derivation of the Dyson equation, and the self-energy calculation in the NCA. The results of numerical solution of the self-consistent system of equations for various hole concentrations and a discussion are presented in Sec. 3. Conclusions are given in Sec. 4.

2. GENERAL FORMULATION

2.1. Effective Hubbard model and Dyson equation

Following the cell-cluster perturbation theory (see, e.g., [19, 22, 23]) based on a consideration of the original two-band p–d model for the CuO_2 layer [24], we consider an effective two-dimensional Hubbard model for holes with the Hamiltonian

$$H = \varepsilon_1 \sum_{i,\sigma} X_i^{\sigma\sigma} + \varepsilon_2 \sum_i X_i^{22} + \sum_{i\neq j,\sigma} \{ t_{ij}^{11} X_i^{\sigma 0} X_j^{0\sigma} + t_{ij}^{22} X_i^{2\sigma} X_j^{\sigma 2} + 2\sigma t_{ij}^{12} (X_i^{2\bar{\sigma}} X_j^{0\sigma} + \text{H.c.}) \}, \quad (1)$$

where $X_i^{nm} = |in\rangle\langle im|$ are the Hubbard operators (HOs) for the four states $n, m = |0\rangle, |\sigma\rangle, |2\rangle = |\uparrow\downarrow\rangle$, $\sigma = \pm 1/2 = (\uparrow, \downarrow)$, $\bar{\sigma} = -\sigma$. Here, $\varepsilon_1 = \varepsilon_d - \mu$ and $\varepsilon_2 = 2\varepsilon_1 + U_{eff}$, where μ is the chemical potential. The effective Coulomb energy in Hubbard model (1) is the charge-transfer energy $U_{eff} = \Delta = \epsilon_p - \epsilon_d$. The respective superscripts 2 and 1 refer to the two-hole p–d singlet subband and the one-hole subband. According to the cell-cluster perturbation theory, we can take similar values for the hopping parameters in (1): $t_{ij}^{22} = t_{ij}^{11} = t_{ij}^{12} = t_{ij}$. We determine the bare electron dispersion defined by the hopping parameter t_{ij} by the conventional equation

$$t(\mathbf{k}) = 4t\gamma(\mathbf{k}) + 4t'\gamma'(\mathbf{k}) + 4t''\gamma''(\mathbf{k}), \quad (2)$$

where t, t', and t'' are the respective hopping parameters for the nearest-neighbor (n.n.) $(\pm a_x, \pm a_y)$, next-nearest-neighbor (n.n.n.) $\pm(a_x \pm a_y)$, and $\pm 2a_x, \pm 2a_y$ sites and $\gamma(\mathbf{k}) = (\cos k_x + \cos k_y)/2$, $\gamma'(\mathbf{k}) = \cos k_x \cos k_y$, and $\gamma''(\mathbf{k}) = (\cos 2k_x + \cos 2k_y)/2$ (the lattice constants $a_x = a_y$ are equal to unity). To obtain a physically reasonable value for the charge-transfer gap for the conventional value $t \approx 0.4$ eV, we take $\Delta = U_{eff} = 8t \approx 3.2$ eV. The bare bandwidth is $W = 8t \approx U_{eff}$, which shows that the effective p–d Hubbard model (1) corresponds to the strong-correlation limit. In what follows, the energy is measured in units of t with $\varepsilon_d = 0$ in ε_1. The chemical

potential μ depends on the average hole occupation number

$$n = 1 + \delta = \left\langle \sum_{\sigma} X_i^{\sigma\sigma} + 2X_i^{22} \right\rangle. \qquad (3)$$

The HOs entering (1) obey the completeness relation $X_i^{00} + X_i^{\uparrow\uparrow} + X_i^{\downarrow\downarrow} + X_i^{22} = 1$, which rigorously preserves the constraint of no double occupancy of any quantum state $|in\rangle$ at each lattice site i. Due to the projected character of the HOs, they have complicated commutation relations $\left[X_i^{\alpha\beta}, X_j^{\gamma\delta}\right]_{\pm} = \delta_{ij}\left(\delta_{\beta\gamma}X_i^{\alpha\delta} \pm \delta_{\delta\alpha}X_i^{\gamma\beta}\right)$, which results in the so-called kinematical interaction. The upper sign here refers to the Fermi-like HOs such as $X_i^{0\sigma}$ and the lower sign is for the Bose-like HOs, such as the spin or number operators.

To discuss the electronic structure within the model in (1), we introduce a thermodynamic matrix Green's function [18]

$$\hat{G}_{ij\sigma}(t-t') = \langle\langle \hat{X}_{i\sigma}(t) \,|\, \hat{X}_{j\sigma}^{\dagger}(t')\rangle\rangle = \\ = -i\theta(t-t')\langle\{\hat{X}_{i\sigma}(t), \hat{X}_{j\sigma}^{\dagger}(t')\}\rangle, \qquad (4)$$

in terms of the two-component operators $\hat{X}_{i\sigma} = \begin{pmatrix} X_i^{\sigma 2} \\ X_i^{0\bar{\sigma}} \end{pmatrix}$ and $\hat{X}_{i\sigma}^{\dagger} = (X_i^{2\sigma}\ X_i^{\bar{\sigma}0})$. To calculate GF (4), we apply the Mori-type projection technique by writing equations of motion for the Heisenberg operators as

$$\hat{Z}_{i\sigma} = [\hat{X}_{i\sigma},\, H] = \sum_j \hat{\varepsilon}_{ij\sigma}\hat{X}_{j\sigma} + \hat{Z}_{i\sigma}^{(ir)}, \qquad (5)$$

where the irreducible $\hat{Z}$-operator is determined by the orthogonality condition

$$\langle\{\hat{Z}_{i\sigma}^{(ir)},\, \hat{X}_{j\sigma}^{\dagger}\}\rangle = \langle\hat{Z}_{i\sigma}^{(ir)}\,\hat{X}_{j\sigma}^{\dagger} + \hat{X}_{j\sigma}^{\dagger}\,\hat{Z}_{i\sigma}^{(ir)}\rangle = 0\,. \qquad (6)$$

This defines the frequency matrix

$$\hat{\varepsilon}_{ij} = \langle\{[\hat{X}_{i\sigma}, H], \hat{X}_{j\sigma}^{\dagger}\}\rangle\hat{Q}^{-1}, \qquad (7)$$

where $\hat{Q} = \langle\{\hat{X}_{i\sigma}, \hat{X}_{i\sigma}^{\dagger}\}\rangle = \begin{pmatrix} Q_2 & 0 \\ 0 & Q_1 \end{pmatrix}$. The weight factors $Q_2 = \langle X_i^{22} + X_i^{\sigma\sigma}\rangle = n/2$ and $Q_1 = \langle X_i^{00} + X_i^{\bar{\sigma}\bar{\sigma}}\rangle = 1 - Q_2$ in a paramagnetic state depend only on the hole occupation number (3). Frequency matrix (7) determines the QP spectra within the generalized mean-field approximation (MFA). The corresponding zero-order GF in the MFA is given by

$$\hat{G}_{\sigma}^{0}(\mathbf{k},\omega) = \left(\omega\hat{\tau}_0 - \hat{\varepsilon}(\mathbf{k})\right)^{-1}\hat{Q}, \qquad (8)$$

where $\hat{\tau}_0$ is the unity matrix and we introduce the frequency matrix (7) in the $\mathbf{k}$-representation $\hat{\varepsilon}(\mathbf{k})$. By differentiating the many-particle GF $\langle\langle \hat{Z}_{i\sigma}^{irr}(t) \,|\, \hat{X}_{j\sigma}^{\dagger}(t')\rangle\rangle$ with respect to the second time t' and applying the same projection procedure as in (5), we derive the Dyson equation as [19]

$$\hat{G}_{\sigma}(\mathbf{k},\omega)^{-1} = \hat{G}_{\sigma}^{0}(\mathbf{k},\omega)^{-1} - \hat{\Sigma}_{\sigma}(\mathbf{k},\omega). \qquad (9)$$

The self-energy matrix $\hat{\Sigma}_{\sigma}(\mathbf{k},\omega)$ is here determined by a proper part (which has no single zero-order GF) of the many-particle GF as

$$\hat{\Sigma}_{\sigma}(\mathbf{k},\omega) = \hat{Q}^{-1}\langle\langle\!\langle \hat{Z}_{\sigma}^{(ir)} \,|\, \hat{Z}_{\sigma}^{(ir)\dagger}\rangle\!\rangle\rangle_{\mathbf{k},\omega}^{(prop)}\ \hat{Q}^{-1}. \qquad (10)$$

Equations (8)–(10) provide an exact representation for GF (4). However, to calculate it, we have to use an approximation for self-energy matrix (10), which describes the inelastic scattering of electrons on spin and charge fluctuations.

It is important to point out that in the Hubbard model in (1), the electron interaction with spin- or charge fluctuations is induced by the kinematical interaction with the coupling constants equal to the original hopping parameters, as has been already pointed out by Hubbard [5]. For instance, the equation of motion for the operator $X_i^{\sigma 2}$ is given by

$$id\,X_i^{\sigma 2}/dt = [X_i^{\sigma 2}, H] = (\varepsilon_1 + \Delta)X_i^{\sigma 2} + \\ + \sum_{l\neq i,\sigma'}\left(t_{il}^{22}B_{i\sigma\sigma'}^{22}X_l^{\sigma' 2} - 2\sigma t_{il}^{21}B_{i\sigma\sigma'}^{21}X_l^{0\bar{\sigma}'}\right) - \\ - \sum_{l\neq i} X_i^{02}\left(t_{il}^{11}X_l^{\sigma 0} + 2\sigma t_{il}^{21}X_l^{2\bar{\sigma}}\right), \qquad (11)$$

where $B_{i\sigma\sigma'}^{\alpha\beta}$ are Bose-like operators describing the number (charge) and spin fluctuations:

$$B_{i\sigma\sigma'}^{22} = (X_i^{22} + X_i^{\sigma\sigma})\delta_{\sigma'\sigma} + X_i^{\sigma\bar{\sigma}}\delta_{\sigma'\bar{\sigma}} = \\ = \left(\frac{N_i}{2} + S_i^z\right)\delta_{\sigma'\sigma} + S_i^{\sigma}\delta_{\sigma'\bar{\sigma}}, \\ B_{i\sigma\sigma'}^{21} = \left(\frac{N_i}{2} + S_i^z\right)\delta_{\sigma'\sigma} - S_i^{\sigma}\delta_{\sigma'\bar{\sigma}}\,. \qquad (12)$$

Therefore, in contrast to spin-fermion models, where the electron interaction with spin or charge fluctuations is specified by fitting coupling constants [3], this interaction is fixed by the hopping parameters in Hubbard model (1).

2.2. Mean-Field approximation

The single-particle excitations in the MFA are defined by frequency matrix (7). Using equations of mo-

tion like (11), we obtain the energy spectrum for holes in two subbands as

$$\varepsilon_{1,2}(\mathbf{k}) = \frac{1}{2}[\omega_2(\mathbf{k}) + \omega_1(\mathbf{k})] \mp \frac{1}{2}\Lambda(\mathbf{k}),$$
$$\Lambda(\mathbf{k}) = \{[\omega_2(\mathbf{k}) - \omega_1(\mathbf{k})]^2 + 4W(\mathbf{k})^2\}^{1/2}, \quad (13)$$

where the original excitation spectra in the Hubbard subbands and the hybridization parameter are

$$\omega_1(\mathbf{k}) = 4t\alpha_1\gamma(\mathbf{k}) + 4t'\beta_1\gamma'(\mathbf{k}) - \mu,$$
$$\omega_2(\mathbf{k}) = 4t\alpha_2\gamma(\mathbf{k}) + 4t'\beta_2\gamma'(\mathbf{k}) + \Delta - \mu, \quad (14)$$
$$W(\mathbf{k}) = 4t\alpha_{12}\gamma(\mathbf{k}) + 4t'\beta_{12}\gamma'(\mathbf{k}),$$

where we omitted the t'' contribution in (2) and introduced the renormalization parameters

$$\alpha_{1(2)} = Q_{1(2)}\left[1+\frac{C_1}{Q^2_{1(2)}}\right], \quad \beta_{1(2)} = Q_{1(2)}\left[1+\frac{C_2}{Q^2_{1(2)}}\right],$$
$$\alpha_{12} = \sqrt{Q_1Q_2}\left[1-\frac{C_1}{Q_1Q_2}\right],$$

and

$$\beta_{12} = \sqrt{Q_1Q_2}\left[1-\frac{C_2}{Q_1Q_2}\right].$$

As in the Hubbard I approximation, we neglect the number fluctuations $\langle\delta N_i\delta N_j\rangle_{(i\neq j)}$ but take the contributions from the spin correlation functions for the n.n. and the n.n.n. sites into account:

$$C_1 = \langle \mathbf{S}_i\mathbf{S}_{i\pm a_x/a_y}\rangle, \quad C_2 = \langle \mathbf{S}_i\mathbf{S}_{i\pm a_x\pm a_y}\rangle. \quad (15)$$

The renormalization of QP spectra (13) and (14) caused by strong spin correlations in the underdoped region results in a suppression of the n.n. hopping, which changes the shape of the spectra and reduces the bandwidth. For instance, if we consider the limit case of the long-range AF Néel state with the n.n. correlation function $C_1 \approx -1/4$ at half-filling, $Q_1 = Q_2 = 1/2$, we obtain $\alpha_{1(2)} = 0$. This results in the complete suppression of the n.n. hopping and the transformation of spectra (14) into the n.n.n. hopping $\propto t'\gamma'(\mathbf{k})$, as was discussed in [19].

For the diagonal components of the zero-order GF in (8), we have

$$G^0_{11(22)}(\mathbf{k},\omega) = \frac{Q_{1(2)}\,[1-b(\mathbf{k})]}{\omega - \varepsilon_{1(2)}(\mathbf{k})} + \frac{Q_{1(2)}\,b(\mathbf{k})}{\omega - \varepsilon_{2(1)}(\mathbf{k})}, \quad (16)$$

where the parameter

$$b(\mathbf{k}) = \frac{\varepsilon_2(\mathbf{k}) - \omega_2(\mathbf{k})}{\varepsilon_2(\mathbf{k}) - \varepsilon_1(\mathbf{k})} = \frac{1}{2} - \frac{\omega_2(\mathbf{k}) - \omega_1(\mathbf{k})}{2\Lambda(\mathbf{k})} \quad (17)$$

determines the contribution due to hybridization.

2.3. Self-energy corrections

Dyson equation (9) for the GF can be conveniently written as

$$\hat{G}_\sigma(\mathbf{k},\omega) = \left(\omega\hat{\tau}_0 - \hat{\varepsilon}(\mathbf{k}) - \tilde{\Sigma}_\sigma(\mathbf{k},\omega)\right)^{-1}\hat{Q}, \quad (18)$$

where the self-energy is given by

$$\tilde{\Sigma}_\sigma(\mathbf{k},\omega) = \langle\langle \hat{Z}^{(ir)}_\sigma \,|\, \hat{Z}^{(ir)\dagger}_\sigma\rangle\rangle^{(prop)}_{\mathbf{k},\omega}\,\hat{Q}^{-1}. \quad (19)$$

In self-energy matrix (19), to make the problem tractable, we can neglect the off-diagonal components $\tilde{\Sigma}_{12,\sigma}(\mathbf{k},\omega)$ in comparison with the hybridization parameters $W(\mathbf{k})$ in (14). This enables us to write the diagonal components of the full GF in (18) in the form similar to (16):

$$\hat{G}_{11(22)}(\mathbf{k},\omega) = \frac{Q_{1(2)}\,[1-b(\mathbf{k})]}{\omega - \varepsilon_{1(2)}(\mathbf{k}) - \tilde{\Sigma}_{11(22)}(\mathbf{k},\omega)} +$$
$$+ \frac{Q_{1(2)}\,b(\mathbf{k})}{\omega - \varepsilon_{2(1)}(\mathbf{k}) - \tilde{\Sigma}_{22(11)}(\mathbf{k},\omega)}, \quad (20)$$

where the hybridization parameters $b(\mathbf{k})$ are determined by the formula similar to (17), which gives an accurate approximation for low doping at $n \sim 1$.

We now calculate self-energy (19) in the noncrossing approximation (NCA) or the self-consistent Born approximation (SCBA) by neglecting vertex renormalization. As follows from equation of motion (11), the $\hat{Z}^{(ir)}_\sigma$ operators determined by (5) are essentially a product of Fermi-like $X_j(t)$ and Bose-like $B_i(t)$ operators. In the SCBA, these excitations of different types in the many-particle GF in (19) are assumed to propagate independently of each other. Therefore, they can be decoupled in the time-dependent correlation functions for lattice sites ($i \neq j$, $l \neq m$) as

$$\langle B_i(t)X_j(t)B_lX_m\rangle \approx \langle X_j(t)X_m\rangle\langle B_i(t)B_l\rangle. \quad (21)$$

Using the spectral representation for these correlation functions, we obtain the following formula for the diagonal self-energy components $\tilde{\Sigma}_{11(22)}(\mathbf{k},\omega) = \Sigma(\mathbf{k},\omega)$ (which are the same for two subbands):

$$\Sigma(\mathbf{k},\omega) = \frac{1}{N}\sum_{\mathbf{q}}\int_{-\infty}^{+\infty} \mathrm{d}z K(\omega,z|\mathbf{q},\mathbf{k}-\mathbf{q}) \times$$
$$\times -\frac{1}{\pi}\,\mathrm{Im}[G_1(\mathbf{q},z) + G_2(\mathbf{q},z)]. \quad (22)$$

The corresponding subband GFs are given by

$$G_{1(2)}(\mathbf{q},\omega) = \frac{1}{\omega - \varepsilon_{1(2)}(\mathbf{q}) - \Sigma(\mathbf{q},\omega)}. \quad (23)$$

The kernel of integral equation (22) has the form

$$K(\omega, z|\mathbf{q}, \mathbf{k}-\mathbf{q}) = |t(\mathbf{q})|^2 \frac{1}{2\pi} \int\limits_{-\infty}^{+\infty} \frac{d\Omega}{\omega - z - \Omega} \times \\ \times \left(\operatorname{th} \frac{z}{2T} + \operatorname{cth} \frac{\Omega}{2T} \right) \operatorname{Im} \chi_{sc}(\mathbf{k}-\mathbf{q}, \Omega), \quad (24)$$

where the interaction is defined by the hopping parameter $t(\mathbf{q})$ in (2). The spectral density of bosonic excitations is determined by the dynamic susceptibility of the Bose-like operators $B_i(t)$ in (21) — the spin and number (charge) fluctuations:

$$\chi_{sc}(\mathbf{q}, \omega) = -\left[\langle\langle \mathbf{S}_\mathbf{q} | \mathbf{S}_{-\mathbf{q}} \rangle\rangle_\omega + \frac{1}{4} \langle\langle \delta N_\mathbf{q} | \delta N_{-\mathbf{q}} \rangle\rangle_\omega \right], \quad (25)$$

where we introduce the commutator GF for the spin $\mathbf{S}_\mathbf{q}$ and the number $\delta N_\mathbf{q} = N_\mathbf{q} - \langle N_\mathbf{q} \rangle$ operators.

We thus obtain a self-consistent system of equations for GFs (23) and self-energy (22). A similar system of equations was obtained within the composite-operator method [16]. In Hubbard model (1), we have two contributions to self-energy (22) determined by the two Hubbard subbands, while in the t–J model studied by us in [20], only one subband is considered. However, depending on the position of the chemical potential, a substantial contribution to the self-energy comes only from the GF of the subband that is close to the Fermi energy. The contribution from the GF of the other subband, which is far from the Fermi energy, is suppressed due to a large charge-transfer energy Δ in the denominator of those GF. Neglecting the latter contribution, we obtain a self-consistent system of equations for one GF close to the Fermi energy and the corresponding self-energy function similar to that in the t–J model [20].

3. RESULTS AND DISCUSSION

3.1. Self-consistent system of equations

To solve the system of equations for self-energy (22) and GFs (23), we must specify a model for the spin-charge susceptibility (25). Below, we take only the spin-fluctuation contribution $\chi_s(\mathbf{q}, \omega) = -\langle\langle \mathbf{S}_q \mid \mathbf{S}_{-q} \rangle\rangle_\omega$ into account, for which we adopt a model suggested in numerical studies [25]:

$$\operatorname{Im} \chi_s(\mathbf{q}, \omega + i0^+) = \chi_s(\mathbf{q})\, \chi_s''(\omega) = \\ = \frac{\chi_0}{1 + \xi^2(1+\gamma(\mathbf{q}))} \operatorname{th} \frac{\omega}{2T} \frac{1}{1 + (\omega/\omega_s)^2}. \quad (26)$$

Static spin correlation functions (29), the coefficient $C(\xi)$ in (30), and the AF correlation length ξ in (26) at various hole concentrations $n = 1 + \delta$

	δ					
	0.03	0.05	0.10	0.15	0.20	0.30
C_1	−0.36	−0.26	−0.21	−0.18	−0.14	−0.10
C_2	0.27	0.16	0.11	0.09	0.06	0.04
$C(\xi)$	22.0	5.91	3.58	2.67	1.93	1.40
ξ	8.0	3.40	2.50	2.10	1.70	1.40

The $\mathbf{q}$-dependence in $\chi_s(\mathbf{q})$ is determined by the AF correlation length ξ, whose doping dependence is defined below. The static susceptibility χ_0 at the AF wave vector $\mathbf{Q} = (\pi, \pi)$ is fixed by the normalization condition

$$\langle \mathbf{S}_i^2 \rangle = \frac{1}{N} \sum_i \langle \mathbf{S}_i \mathbf{S}_i \rangle = \\ = \frac{1}{\pi} \int\limits_{-\infty}^{\infty} \frac{dz}{\exp(z/T) - 1} \chi_s''(z) \frac{1}{N} \sum_\mathbf{q} \chi_s(\mathbf{q}), \quad (27)$$

which gives the following value for this constant:

$$\chi_0 = \frac{2}{\omega_s} \langle \mathbf{S}_i^2 \rangle \left\{ \frac{1}{N} \sum_\mathbf{q} \frac{1}{1 + \xi^2[1 + \gamma(\mathbf{q})]} \right\}^{-1}. \quad (28)$$

In (27), we introduce

$$\langle \mathbf{S}_i^2 \rangle = 3\langle S_i^z S_i^z \rangle = \frac{3}{4} \langle (1 - X_i^{00} - X_i^{22}) \rangle = \frac{3}{4}(1 - |\delta|),$$

where $\delta \approx \langle X_i^{22} \rangle$ at the hole doping and $\delta \approx -\langle X_i^{00} \rangle$ at the electron doping.

Spin correlation functions (15) in single-particle excitation spectra (13) in the MFA are defined by equations

$$C_1 = \frac{1}{N} \sum_\mathbf{q} C_\mathbf{q}\, \gamma(\mathbf{q}), \quad C_2 = \frac{1}{N} \sum_\mathbf{q} C_\mathbf{q}\, \gamma'(\mathbf{q}). \quad (29)$$

The static correlation function $C_\mathbf{q}$ can be calculated from the same model (26) as

$$C_\mathbf{q} = \langle \mathbf{S}_\mathbf{q} \mathbf{S}_{-\mathbf{q}} \rangle = \frac{C(\xi)}{1 + \xi^2[1 + \gamma(\mathbf{q})]}, \quad (30)$$

where $C(\xi) = \chi_0 (\omega_s/2)$.

To specify the doping dependence of the AF correlation length $\xi(\delta)$ at low temperature, we fit the correlation function C_1 calculated from (29) to the numerical results of an exact diagonalization for finite clusters [26]. The values of the AF correlation length, the

calculated values of C_2, and the correlation function $C(\xi) = \langle \mathbf{S_q S_{-q}} \rangle$ at the AF wave vector $\mathbf{q} = \mathbf{Q} = (\pi, \pi)$ are given in the Table.

To perform numerical calculations, we introduce the imaginary frequency representation for GF (23):

$$G_{1(2)}(\mathbf{q}, i\omega_n) = \frac{1}{i\omega_n - \varepsilon_{1(2)}(\mathbf{q}) - \Sigma(\mathbf{q}, i\omega_n)}, \qquad (31)$$

where $i\omega_n = i\pi T(2n+1)$, $n = 0, \pm 1, \pm 2, \ldots$ For self-energy (22), we obtain the representation

$$\Sigma(\mathbf{k}, i\omega_n) = -\frac{T}{N} \sum_{\mathbf{q}} \sum_{m} [G_1(\mathbf{q}, i\omega_m) + G_2(\mathbf{q}, i\omega_m)] \times \\ \times \lambda(\mathbf{q}, \mathbf{k}-\mathbf{q} \mid i\omega_n - i\omega_m). \qquad (32)$$

The interaction function is given here by the equation

$$\lambda(\mathbf{q}, \mathbf{k}-\mathbf{q} \mid i\omega_\nu) = -|t(\mathbf{q})|^2 \, \chi_s(\mathbf{k}-\mathbf{q}) \, F_s(i\omega_\nu) \qquad (33)$$

with the spectral function

$$F_s(\omega_\nu) = \frac{1}{\pi} \int_0^\infty \frac{2x dx}{x^2 + (\omega_\nu/\omega_s)^2} \, \frac{1}{1+x^2} \, \mathrm{th} \, \frac{x\omega_s}{2T}. \qquad (34)$$

We compare the self-consistent system of equations for GF (31) and self-energy (32) with the results of other theoretical approaches. In our theory based on the HO technique, we start from the two-subband representation for GF (4), which rigorously takes strong electron correlations determined by the Coulomb energy U_{eff} into account. This results in the Mott gap at large U_{eff} (see below) as in the DMFT. On the other hand, the kinematical interaction, generic to HOs, induces the electron scattering by spin (charge) dynamical fluctuations (25), which are responsible for the pseudogap formation as in the two-particle self-consistent approach (TPSC) [12, 27] or the model of short-range static spin (charge) fluctuations (the $\Sigma_{\mathbf{k}}$-model) [2].

To prove this, we consider the classical limit for self-energy (32) by taking only the zero Matsubara frequency $i\omega_\nu = 0$ into account in the interaction (33), which gives $i\omega_m = i\omega_n$ in (32). In the limit of a large AF correlation length $\xi \gg 1$, the static spin susceptibility $\chi_s(\mathbf{q})$ in (26) shows a sharp peak close to the AF wave-vector $\mathbf{Q} = (\pi, \pi)$ and can be expanded in the small wave vector $\mathbf{p} = \mathbf{q} - \mathbf{Q}$:

$$\chi_s(\mathbf{q}) \approx \frac{\chi_0}{1 + \xi^2 \mathbf{p}^2} \approx \frac{A}{\kappa^2 + \mathbf{p}^2}, \qquad (35)$$

where we introduce $\kappa = \xi^{-1}$ and take into account that the constant in (28) is given by $\chi_0 \approx A\,\xi^2$ with $A = (8\pi/\omega_s)\langle \mathbf{S}_i^2 \rangle [\ln(1 + 4\pi\,\xi^2)]^{-1}$ for the square lattice. In this limit, we obtain the equation for self-energy (32)

$$\Sigma(\mathbf{k}, i\omega_n) \approx |g(\mathbf{k}-\mathbf{Q})|^2 \, \frac{T}{N} \sum_{\mathbf{p}} \frac{1}{\kappa^2 + p^2} \times \\ \times [G_1(\mathbf{k}-\mathbf{Q}-\mathbf{p}, i\omega_n) + G_2(\mathbf{k}-\mathbf{Q}-\mathbf{p}, i\omega_n)] \qquad (36)$$

with the effective interaction

$$|g(\mathbf{q})|^2 = A \, |t(\mathbf{q})|^2 \, F_s(0). \qquad (37)$$

Expanding the QP energy $\varepsilon_{1(2)}(\mathbf{k}-\mathbf{Q}-\mathbf{p}) \approx \varepsilon_{1(2)}(\mathbf{k}-\mathbf{Q}) - \mathbf{p} \cdot \mathbf{v}_{1(2),\mathbf{k}-\mathbf{Q}}$, we obtain the representation for the GFs in (36) as

$$G_{1(2)}(\mathbf{k}-\mathbf{Q}-\mathbf{p}, i\omega_n) \approx \{ i\omega_n - \varepsilon_{1(2)}(\mathbf{k}-\mathbf{Q}) + \\ + \mathbf{p} \cdot \mathbf{v}_{1(2),\mathbf{k}-\mathbf{Q}} - \Sigma(\mathbf{k}-\mathbf{Q}, i\omega_n) \}^{-1}. \qquad (38)$$

The system of equations for GFs (38) and self-energy (36) is similar to the systems derived in the TPSC approach [27] and the $\Sigma_{\mathbf{k}}$-model [2], apart from the interaction function and the two-subband system of equations. In our approach, vertex (37) is determined by the hopping parameter $|t(\mathbf{k}-\mathbf{Q})|^2$, while in the TPSC and the $\Sigma_{\mathbf{k}}$-model, the coupling constant is induced by the Coulomb scattering, e.g., $g^2 = U^2(\langle n_{i\uparrow} n_{i\downarrow} \rangle / n^2) \langle \mathbf{S}_i^2 \rangle / 3$ in [15]. However, the values of these vertices are close: the value $\langle \sqrt{|t(\mathbf{k})|^2} \rangle_{\mathbf{k}} \sim 2t$ averaged over the BZ is comparable to the coupling constant $g \leq 2t$ used in [13]. In the spin-fermion model, the self-energy is also determined by spin fluctuations (see, e.g., [3]) with the coupling constant fitted from ARPES experiments $g \sim 0.7$ eV$\sim 2t$ of the same order. As in the TPSC theory, in the limit as $\xi \to \infty$, the AF gap $\Delta_{AF}(\mathbf{k}) \propto |t(\mathbf{k}-\mathbf{Q})|^2$ emerges in the QP spectra in the subband located at the Fermi energy. This result readily follows from the self-consistent equations for GFs (31) with self-energy (36), where in the right-hand side, the GF in (38) is taken at $\mathbf{p} = 0$. Thus, the pseudogap formation is mediated in our approach by the AF short-range order similar to the TPSC theory and the model of short-range static spin fluctuations in the generalized DMFT [15].

In what follows, we consider the results of self-consistent calculations of GFs (31) and self-energy (32) in the hole-doped case for various hole concentrations $\delta = n - 1 > 0$. In Secs. 3.2–3.4, the calculations are performed at the temperature $T = 0.03t \approx 140$ K and $T = 0.3t$ for $\Delta = 8t$, $t \approx 0.4$ eV, and $t' = -0.3t$. Several results are reported for $\Delta = 4t$, $t' = -0.13t$, and $t'' = 0.16t$ in Sec. 3.5. For the spin-fluctuation energy in (26), we take $\omega_s = 0.4t$. The AF correlation length $\xi(\delta)$ and the static correlation functions C_1 and C_2 in (15) are defined in the Table.

3.2. Dispersion and spectral functions

In ARPES measurements and QMC simulations, the spectrum of single-electron excitations is determined by the spectral function $A_{(el)}(\mathbf{k},\omega) = A_{(h)}(\mathbf{k},-\omega)$. The spectral function for holes can be written as

$$A_{(h)}(\mathbf{k},\omega) = -\frac{1}{\pi}\,\mathrm{Im}\langle\langle a_{\mathbf{k}\sigma} \mid a^{\dagger}_{\mathbf{k}\sigma}\rangle\rangle_{\omega+i0^{+}} =$$

$$= [Q_1 + P(\mathbf{k})]A_1(\mathbf{k},\omega) + [Q_2 - P(\mathbf{k})]A_2(\mathbf{k},\omega), \quad (39)$$

where we define the hole annihilation $a_{\mathbf{k}\sigma}$ and creation $a^{\dagger}_{\mathbf{k}\sigma}$ operators in terms of the Hubbard operators as $a_{\mathbf{k}\sigma} = X_i^{0\sigma} + 2\sigma X_i^{\bar{\sigma}2}$ and $a^{\dagger}_{\mathbf{k}\sigma} = X_i^{\sigma 0} + 2\sigma X_i^{2\bar{\sigma}}$, and use all the four components of the matrix GF $\hat{G}_{\alpha\beta}(\mathbf{k},\omega)$ in (18) with the diagonal components given by (20). In (39), we also introduce the one-band spectral functions determined by GFs (23):

$$A_{1(2)}(\mathbf{k},\omega) = -\frac{1}{\pi}\,\mathrm{Im}\,G_{1(2)}(\mathbf{q},\omega).$$

The hybridization effects are taken into account by the parameter

$$P(\mathbf{k}) = (n-1)b(\mathbf{k}) - 2\sqrt{Q_1 Q_2}\,\frac{W(\mathbf{k})}{\Lambda(\mathbf{k})}.$$

The dispersion curves given by maxima of spectral functions (39) were calculated for the hole doping $\delta = 0.05-0.3$. At the low hole doping $\delta = 0.05$, 0.1, the dispersion reveal a rather flat hole-doped band at the Fermi energy ($\omega = 0$), as shown in the upper panel in Fig. 1. The corresponding spectral function (the bottom panel) demonstrates weak QP peaks at the Fermi energy. With doping, the dispersion and the intensity of the QP peaks at the Fermi energy substantially increase, as demonstrated in Fig. 2, although a flat band in the $X(\pi,0) \to \Gamma(0,0)$ direction is still observed in agreement with ARPES measurements in the overdoped $La_{1.78}Sr_{0.22}CuO_4$ [28]. To study the influence of AF spin correlations on the spectra, we calculate the spectral functions at the high temperature $T = 0.3t$ for $\delta = 0.1$ by neglecting spin correlation functions (15) in single-particle excitation spectra (13) in the MFA and taking the small AF correlation length $\xi = 1.0$ in the spin susceptibility (26). Figure 3 shows a strong increase in the dispersion and the intensity of the QP peaks at the Fermi energy as in the overdoped region, $\delta = 0.3$, which proves a strong influence of the AF spin correlations on the spectra. A crude estimation of the Fermi velocity from the dispersion curve in the

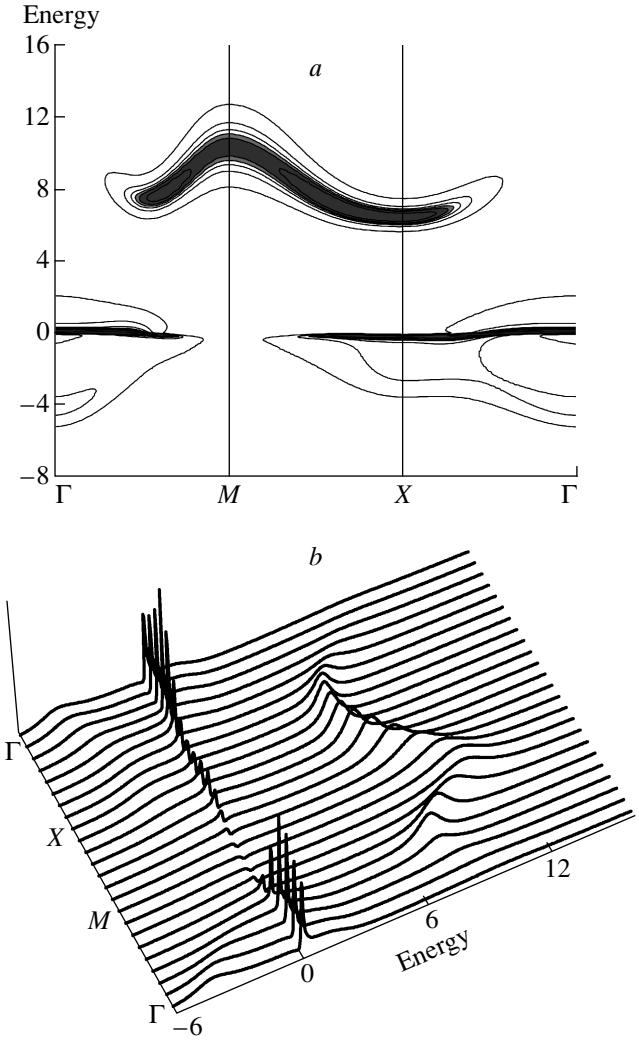

Fig. 1. Dispersion curves (a) and spectral functions (b) in units of t along the symmetry directions $\Gamma(0,0) \to M(\pi,\pi) \to X(\pi,0) \to \Gamma(0,0)$ for $\delta = 0.05$

$\Gamma(0,0) \to M(\pi,\pi)$ direction in Fig. 2 for the overdoped case gives the value $V_F \approx 7.5t$ Å ≈ 3 (eV·Å) for the hopping parameter $t = 0.4$ eV, which can be compared with the experimental results $V_F \approx 2.2$ (eV·Å) for overdoped $La_{1.78}Sr_{0.22}CuO_4$ [28] and $V_F \approx 3.9$ (eV·Å) for overdoped Bi-2212 [29]. With doping, the electron density of states (DOS) shows a weight transfer from the upper one-hole subband to the lower two-hole singlet subband, as shown in Fig. 4. But even in the overdoped case, a noticeable part of the DOS retains in the upper one-hole subband.

It is interesting to compare our results with those obtained in the generalized DMFT [13], which should be close to each other as discussed at the end of Sec. 3.1.

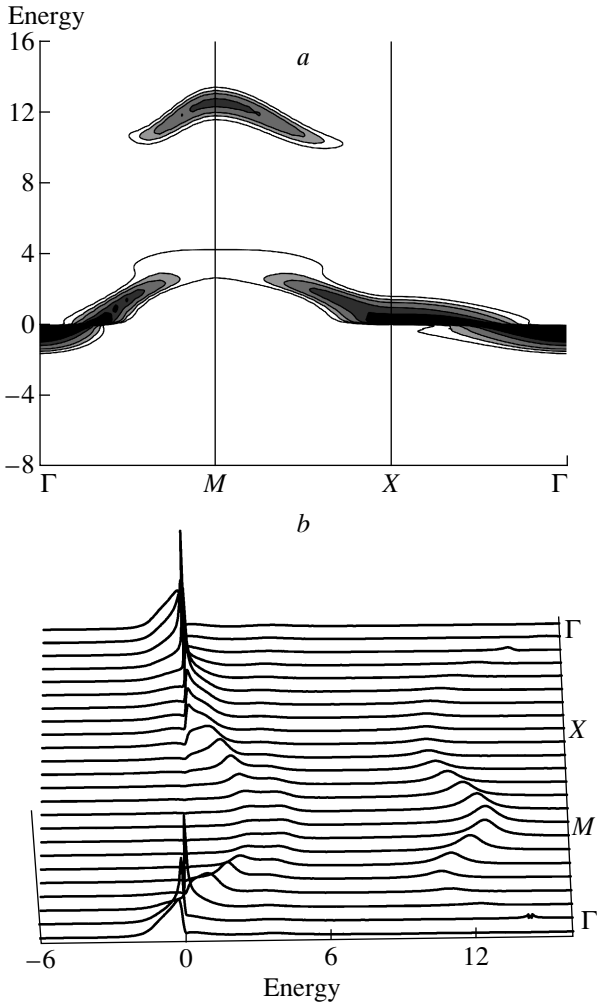

Fig. 2. The same as in Fig. 1 for the hole concentration $\delta = 0.3$

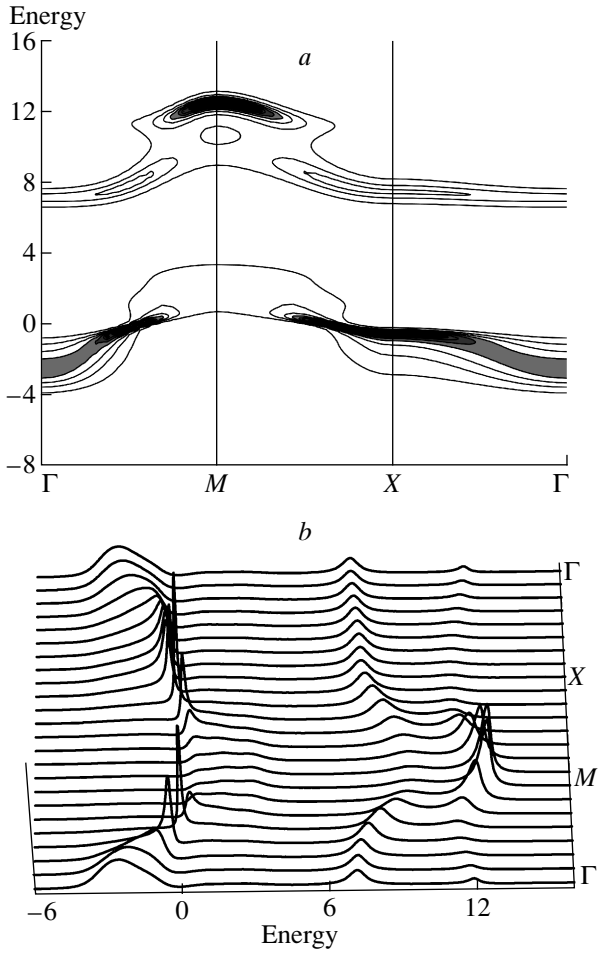

Fig. 3. The same as in Fig. 1 but for the hole concentration $\delta = 0.1$ and at the high temperature $T = 0.3t$

In fact, the spectral function shown in Fig. 8 in [13] for $t' = -0.4$ demonstrates a similar flat QP bands in the $\Gamma(0,0) \to X(\pi,0)$ and $\Gamma(0,0) \to M(\pi,\pi)$ directions, as in our Fig. 1 and Fig. 2, a strong intensity transfer from the lower electronic Hubbard band (LHB) to the upper Hubbard band (UHB) at the $M(\pi,\pi)$ point of the BZ and a splitting of the LHB close to the $X(\pi,0)$ point. An analogous temperature and doping (ξ) behavior of the spectral functions and the pseudogap revealed in both theories supports the spin-fluctuation scenario of the pseudogap formation. A similar behavior was also observed in the cluster perturbation theory [12] (see Fig. 2*a* in [31]).

3.3. Fermi surface and occupation numbers

The Fermi surface for the two-hole subband was determined by the conventional equation

$$\varepsilon_2(\mathbf{k}_{\rm F}) + \mathrm{Re}\,\Sigma(\mathbf{k}_{\rm F}, \omega = 0) = 0, \qquad (40)$$

as shown in Fig. 5, and was then compared with those obtained from maxima of the spectral function $A_{el}(\mathbf{k}, \omega = 0)$ on the (k_x, k_y)-plane for $\delta = 0.1, 0.2$ shown in Fig. 6. The FS changes from a hole arc-type at $\delta = 0.1$ to an electron-like one at $\delta = 0.3$. Experimentally, an electron-like FS was observed in the overdoped $La_{1.78}Sr_{0.22}CuO_4$ [28]. The doping-dependent FS transformation can also be observed by studying the electron occupation numbers. The electron occupation numbers in the $(\mathbf{k})$-space for one spin direction equal to $N_{(el)}(\sigma, \mathbf{k}) = 1 - N_{(h)}(\sigma, \mathbf{k})$, where the hole occupation numbers $N_{(h)}(\sigma, \mathbf{k}) \equiv N_{(h)}(\mathbf{k})$ in accordance

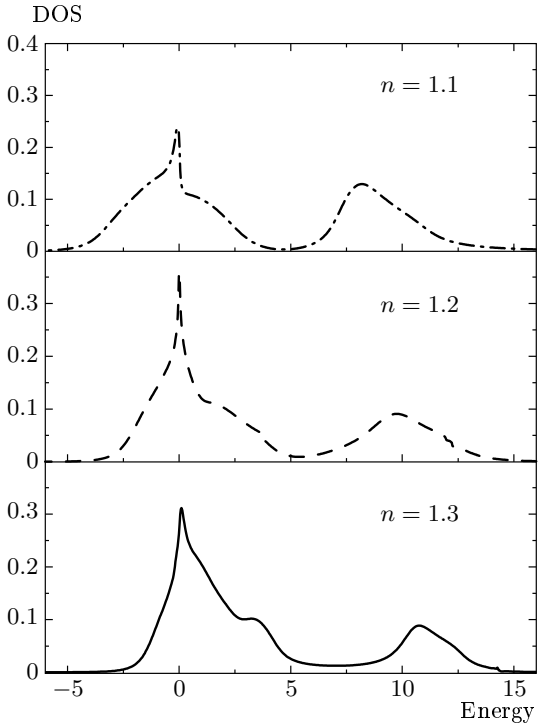

Fig. 4. Doping dependence of the electron density of states

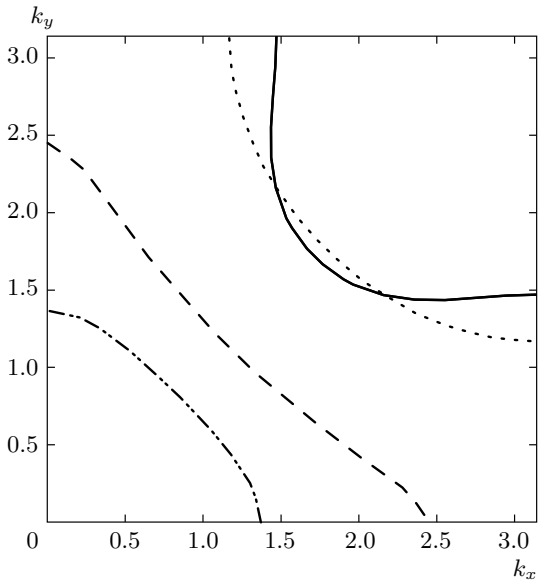

Fig. 5. Doping dependence of the FS for $\delta = 0.1$ (solid line at $T = 0.03t$ and dotted line at $T = 0.3t$), $\delta = 0.2$ (dashed line), and $\delta = 0.3$ (dot-dashed line)

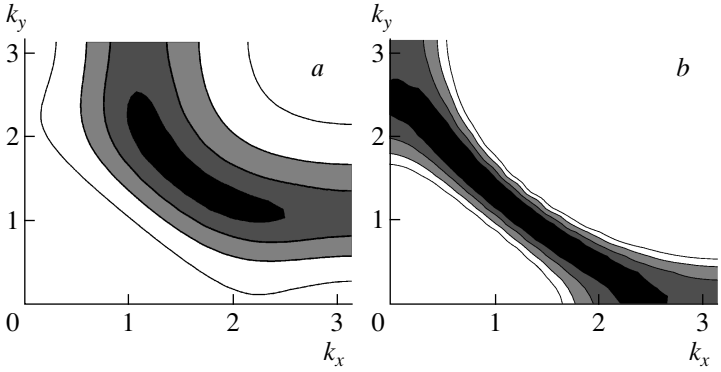

Fig. 6. $A(\mathbf{k}, \omega = 0)$ on the FS for $\delta = 0.1$ (a), $\delta = 0.2$ (b)

with (3), are determined only by diagonal GFs (20). From the last equation and (23), we obtain

$$N_{(h)}(\mathbf{k}) = [Q_1 + (n-1)b(\mathbf{k})]\, N_1(\mathbf{k}) + [Q_2 - (n-1)b(\mathbf{k})]\, N_2(\mathbf{k}),$$

$$N_{1(2)}(\mathbf{k}) = -\frac{1}{\pi}\int\limits_{-\infty}^{\infty} \frac{d\omega}{e^{\omega/T}+1}\, \mathrm{Im}\, G_{1(2)}(\mathbf{k}, \omega) = \frac{1}{2} + \frac{T}{2}\sum_{m=-\infty}^{\infty} G_{1(2)}(\mathbf{k}, i\omega_m). \quad (41)$$

The electron occupation numbers in a quarter of the BZ ($0 < k_x, k_y < \pi$) are shown in Fig. 7 for $\delta = 0.1$ at the low temperature $T = 0.03t$ and at the high temperature $T = 0.3t$. With doping, the shape of $N_{\mathbf{k}}$ changes, revealing a transition of the hole-like FS to the electron-like one in the overdoped case $\delta = 0.3$ as plotted in Fig. 8.

In the underdoped case at $\delta = 0.1$, the decrease in the occupation numbers at the Fermi level crossing is rather small, $\Delta N_{(el)} \approx 0.15$, but for the high temperature $T = 0.3t$ or in the overdoped case at $\delta = 0.3$, when the AF spin correlations are suppressed, the occupation number decrease is much larger: $\Delta N_{(el)} \approx 0.45$ and 0.55, respectively. Therefore, the arc formation and a small change of the electron occupation numbers at the FS crossing at low doping further prove a large contribution of the spin correlations to the renormalization of QP spectra.

The obtained result concerning the "destruction" of the FS caused by the arc formation shown in Figs. 6 and 16 for low doping, which corresponds to large ξ, correlates well with the studies within the generalized DMFT [14]. As shown in Fig. 2 in [14], the spectral density intensity plots clearly demonstrate the arc

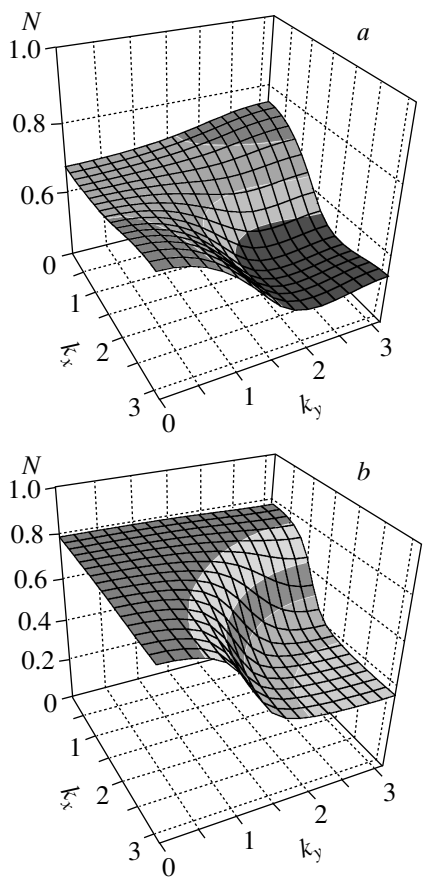

Fig. 7. The electron occupation numbers $N_{\mathbf{k}}$ for $\delta = 0.1$ at $T = 0.03t$ (a) and at $T = 0.3t$ (b)

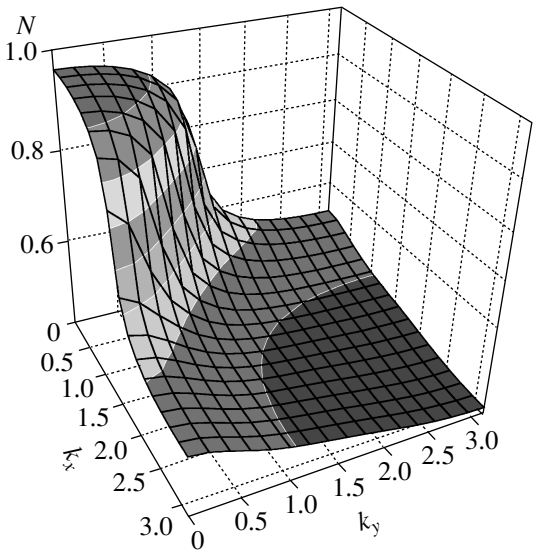

Fig. 8. The electron occupation numbers $N_{\mathbf{k}}$ at $T = 0.03t$ for $\delta = 0.3$

formation on the FS for the large coupling constant $\lambda_{sf} = \Delta = 2t$ and $\xi = 10$, while the FS determined from (40) gives several solutions as in our Fig. 15 for $U_{eff} = 4\,t$ in Sec. 3.5.

3.4. Self-energy and kinks

The energy dependence of the real and imaginary parts of the self-energy $\Sigma(\mathbf{k}, \omega)$ for $\delta = 0.1, 0.3$ at the $\Gamma(0,0)$, $S(\pi/2, \pi/2)$, and $M(\pi, \pi)$ points is shown in Fig. 9. These plots demonstrate a strong dependence of the self-energy on the wave vector and the hole concentrations. With doping, the coupling constant substantially decreases, as can be seen by the decrease in the imaginary part and the slope of the real part at the FS crossing, which determines the coupling constant $\lambda = -(\partial\, \mathrm{Re}\, \tilde{\Sigma}(\mathbf{k}, \omega)/\partial\omega)_{\omega=0}$. As shown in Fig. 10, the coupling constant in the $\Gamma(0,0) \to M(\pi,\pi)$ direction decreases from $\lambda \approx 7.86$ at $\delta = 0.1$ to $\lambda \approx 3.3$ at $\delta = 0.3$. At large binding energies (greater than the boson energy responsible for the interaction), the self-energy effects vanish and the electron dispersion should return to the bare value, giving a sharp bend, the so-called "kink" in the electron dispersion. The amplitude of the kink and the energy scale where it occurs are related to the strength of the electron–boson interaction and the boson energy, respectively. In ARPES experiments, the kink is observed as a change in the slope of the intensity plot for the spectral function $A(\mathbf{k}, \omega)$ in a particular $\mathbf{k}$-wave vector direction below the Fermi level $\omega \leq 0$ (for electrons). Two directions are usually studied: the nodal ($\Gamma \to M$) and the antinodal ($X \to M$) ones. Intensity plots for the spectral function $A(\mathbf{k}, \omega)$ at $\delta = 0.1$ are shown in Fig. 11 in the nodal direction (a) and the antinodal one (b). The same plots at $\delta = 0.3$ are shown in Fig. 12 in the nodal direction (a) and the $X(\pi, 0) \to \Gamma(0,0)$ direction (b). A change in dispersion is clearly seen with increasing the binding energy below the FS shown by dotted line. In the underdoped case, the kink is larger than in the overdoped one. A crude estimation of the strength of the kink from the ratio of the dispersion slope V_{F} close to the FS ($\omega = 0$) to V_{F}^0 at a large binding energy ($\omega \sim 0.2t$), $V_{\mathrm{F}}^0/V_{\mathrm{F}} = (1 + \lambda)$, gives the values $(1 + \lambda) \approx 7.6, 3.5$ at $\delta = 0.1$ for the nodal and antinodal directions, respectively. In the overdoped case, the nodal value is much smaller, while in the antinodal $X(\pi, 0) \to \Gamma(0,0)$ direction, it is still quite large: $(1 + \lambda) \approx 2.5$. These estimations agree with the evaluation of the coupling constant λ from the slope of the real part of the self-energy discussed above.

It is important to stress that in our theory, the

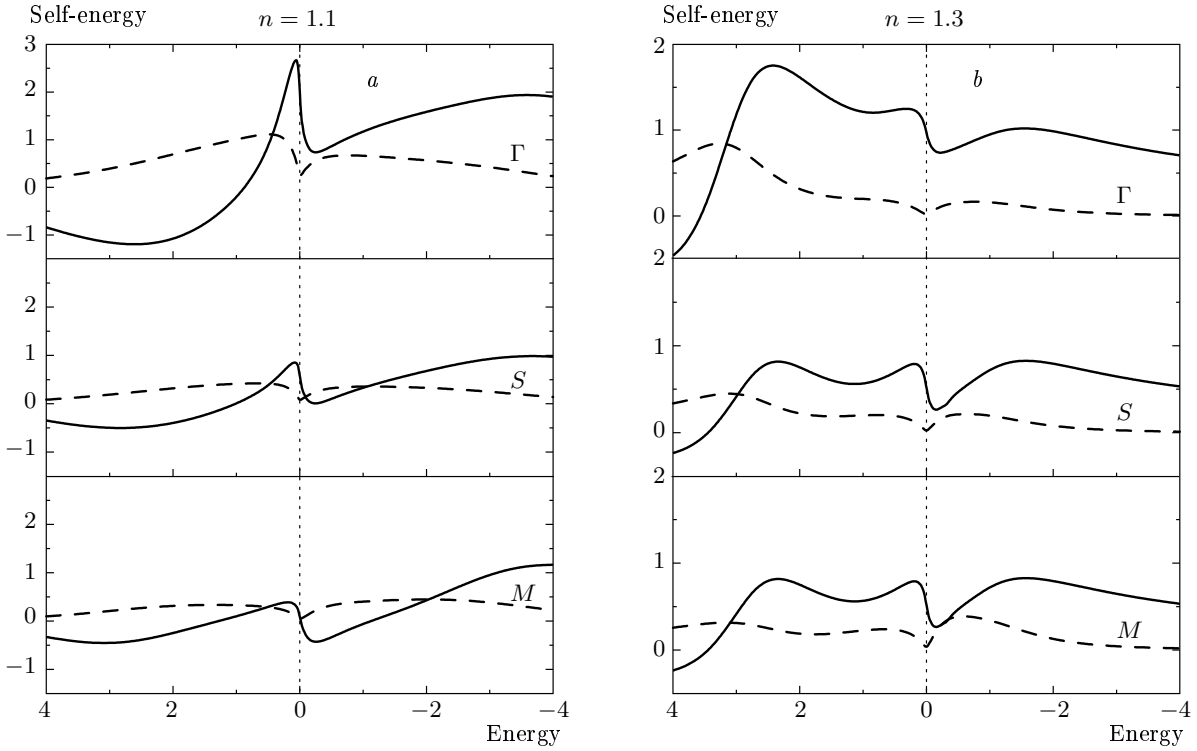

Fig. 9. Energy dependence of the real and imaginary parts of the self-energy $\Sigma(\mathbf{k},\omega)$ at the $\Gamma(0,0)$, $S(\pi/2,\pi/2)$, and $M(\pi,\pi)$ points at $\delta = 0.1$ (a) and $\delta = 0.3$ (b)

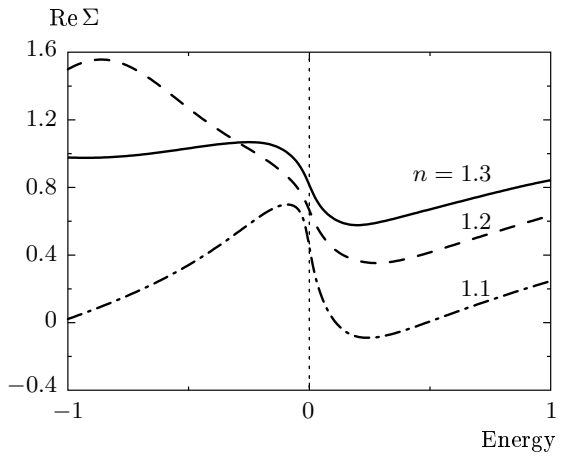

Fig. 10. $Re\Sigma(\mathbf{k},\omega)$ in the $\Gamma(0,0) \to M(\pi,\pi)$ direction at the FS

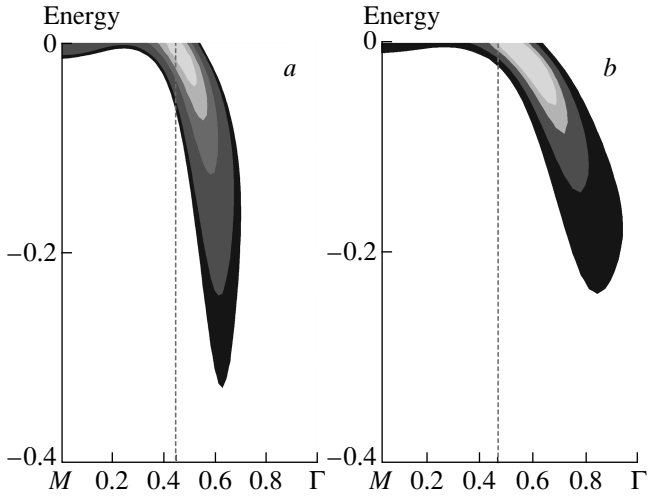

Fig. 11. Dispersion curves along the symmetry directions $M(\pi,\pi) \to \Gamma(0,0)$ (a) and $M(\pi,\pi) \to X(\pi,0)$ (b) in units of t for $\delta = 0.1$, $T = 0.03t$. Fermi level crossing is shown by the vertical dotted line

self-energy effects and the corresponding kinks are induced by the spin-fluctuation spectrum in the form of the continuum (26), which at a low temperature $T \sim 0.03t \ll \omega_s = 0.4t$ has a large intensity already at the small energy $\omega \sim 0.03t$ and decreases slowly up to a high energy $\omega \sim t$. In the spin-fermion model, the kink phenomenon is usually explained by the electron inter-

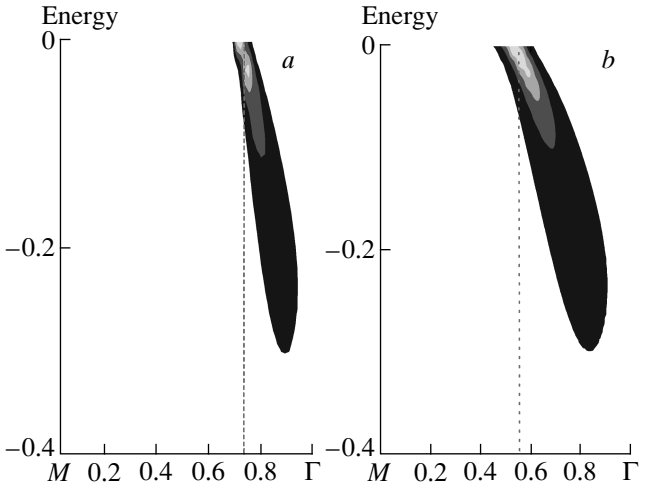

Fig. 12. The same as in Fig. 11 but for $\delta = 0.3$ along the symmetry directions $M(\pi,\pi) \to \Gamma(0,0)(a)$ and $X(\pi,0) \to \Gamma(0,0)$ (b)

action with the spin-resonance mode $\Omega_{\rm res} \approx 40$ meV observed in the superconducting state. This results in a break of the electron dispersion ("kink") at a certain energy $\omega \sim \Omega_{res} + \Delta_0$, where Δ_0 is the superconducting gap (see, e.g., [3]). In the normal state considered in our theory, the spin-resonance mode is inessential. Its contribution amounting to only few percent of the total spin fluctuation spectrum in (27) should not change our results, which reveal a rather strong interaction with a smooth energy variation without any specific kink energy.

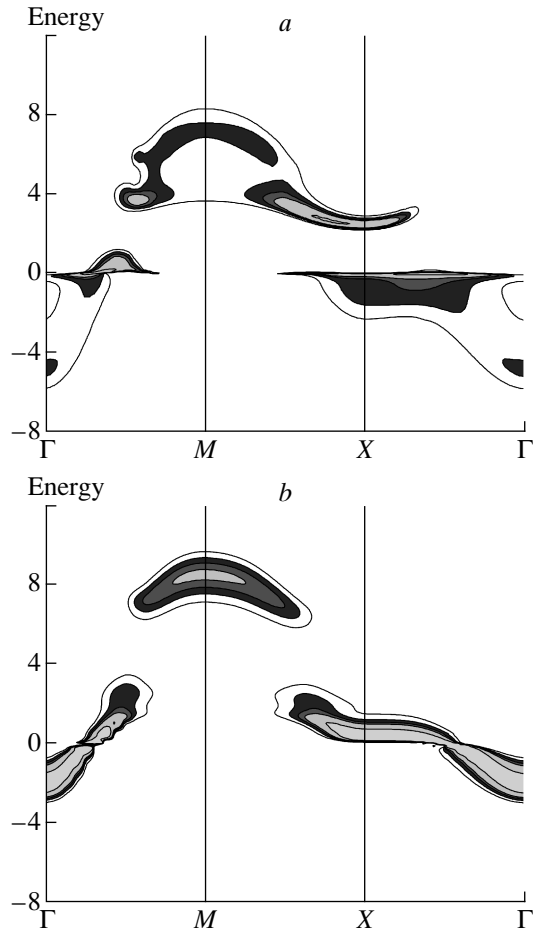

Fig. 13. Dispersion curves for $\Delta = 4t$ along the symmetry directions $\Gamma(0,0) \to M(\pi,\pi) \to X(\pi,0) \to \Gamma(0,0)$ at $\delta = 0.05$ (a) and $\delta = 0.3$ (b)

3.5. Dispersion and FS at $U_{eff} = \Delta = 4t$

The effective Coulomb energy $U_{eff} = 8t$ in the Hubbard model in (1) results in the large charge-transfer gap $\Delta \approx 3$ eV for $t = 0.4$ eV even in the overdoped case, Fig. 2, while experiments point to a smaller value of the order of 1.5–2 eV. In this section, to correct this inconsistency, we present the results obtained for a smaller value $U_{eff} = \Delta = 4t$. We also take the hopping parameter for the n.n.n. $\pm 2a_x, \pm 2a_y$ sites into account and fix the hopping parameter in the model dispersion (2) as suggested for the effective Hubbard model based on the tight-binding fitting of the LDA calculations for La_2CuO_4 [30] as $t' = -0.13t$ and $t'' = 0.16t$ with $t \approx 0.7$ eV.

The main results for the dispersion and the spectral functions do not change much in comparison with the previous ones, as shown in Fig. 13. A larger hybridization between the subbands at small values of U_{eff} results in an increase in the dispersion and the intensity of the upper one-hole subband. This trend is also seen in the DOS in Fig. 14. At weak doping, the Mott gap between the subbands is observed despite the intermediate Coulomb energy value $U_{eff} = 4t$, only a half of the bare bandwidth $W \approx 8t$. This can be explained by a reduction of the bandwidth caused by strong spin correlations in the underdoped region up to $\tilde{W} \sim 8|t'|$, as discussed in Sec. 2.2, below Eq. (15). In the overdoped case at $\delta = 0.3$, when the spin correlations become weak, the gap between the subbands vanishes.

Noticeable changes are observed for the FS shown in Figs. 15 and 16. In the first plot, where the FS was determined by Eq. (40), we see a large pocket at the small doping $\delta = 0.1$, which opens as the doping or temperature increases. At the overdoping for $\delta = 0.3$, the FS transforms to the electron-like one, as in the previous calculations. This transformation is confirmed by

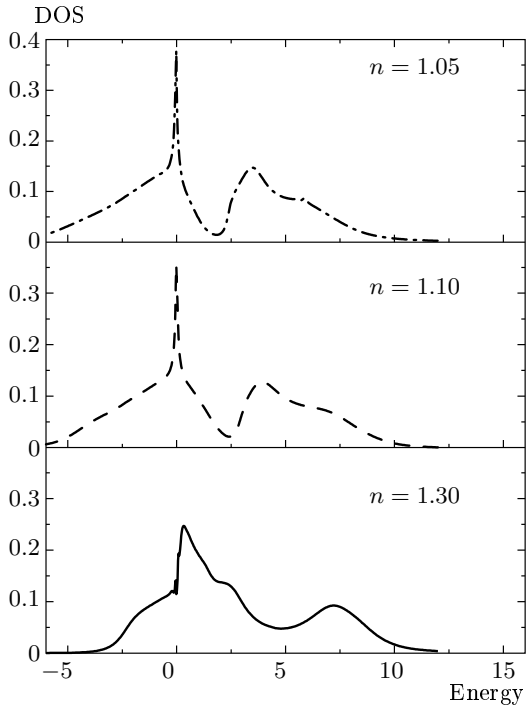

Fig. 14. Doping dependence of the DOS for $\Delta = 4t$

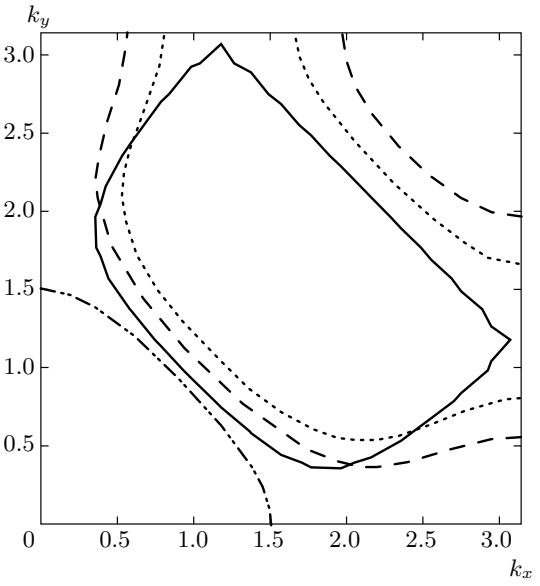

Fig. 15. Doping dependence of the FS for $\delta = 0.1$ (solid line at $T = 0.03t$ and dotted line at $T = 0.3t$), $\delta = 0.2$ (dashed line), and $\delta = 0.3$ (dot-dashed line) for $\Delta = 4t$

calculations of the electron occupation numbers shown in Fig. 17. We note that a pronounced hole pocket in the new set of the model parameters is caused by the t'' contribution, which results in a large dispersion in the $(\pi, 0) \to (0, \pi)$ direction ($\propto t''(\cos 2k_x + \cos 2k_y)$), disregarded in the previous set of the parameters. A remarkable feature of these results is that the part of the FS close to the $\Gamma(0, 0)$ point in the nodal direction in Fig. 15 does not shift much with doping (or temperature), being pinned to a large FS as observed in ARPES experiments (see, e.g., [29]). In fact, only this part of the FS was detected in the ARPES experiments, where the spectral function $A_{el}(\mathbf{k}, \omega = 0)$ shown in Fig. 16 was measured.

The self-energy effects and kinks are similar to those for $\Delta = 8t$ and confirm a strong influence of spin correlations on the QP spectra renormalization. As shown in Fig. 18, the coupling constant $\lambda = -(\partial \operatorname{Re} \tilde{\Sigma}(\mathbf{k}, \omega)/\partial\omega)_{\omega=0}$, being large at small doping, distinctly decreases with overdoping at $\delta = 0.3$, which is accompanied by suppression of the imaginary part of the self-energy. In conclusion, the alternative set of parameters with a moderate effective Coulomb energy $U_{eff} = 4t$ in Hubbard model (1) confirms the important role played by AF correlations in the electronic structure of the system with a large single-site Coulomb interaction.

4. CONCLUSION

We have formulated the theory of electron spectra in the strong-correlation limit for Hubbard model (1) in a paramagnetic state. Using the Mori-type projection technique for the thermodynamic GFs in terms of the Hubbard operators, we consistently took charge carrier scattering by dynamical spin fluctuations into account and derived the self-consistent system of equations for GFs (23) and self-energy (22) evaluated in the NCA, which neglects the vertex corrections. Although the electron coupling to spin fluctuations is not weak in Hubbard model (1), being of the order of the hopping parameter, the vertex corrections should not be very important in this case due to kinematical restrictions imposed on the spin-fluctuation scattering. As was shown for the t–J model [32], the leading two-loop crossing diagram identically vanishes, while the next three-loop crossing diagram gives a small contribution to the self-energy. In any case, the NCA for the self-energy can be considered a starting approximation for a model with strong coupling. As discussed at the end of Sec. 3.1, the self-consistent systems of equations for the

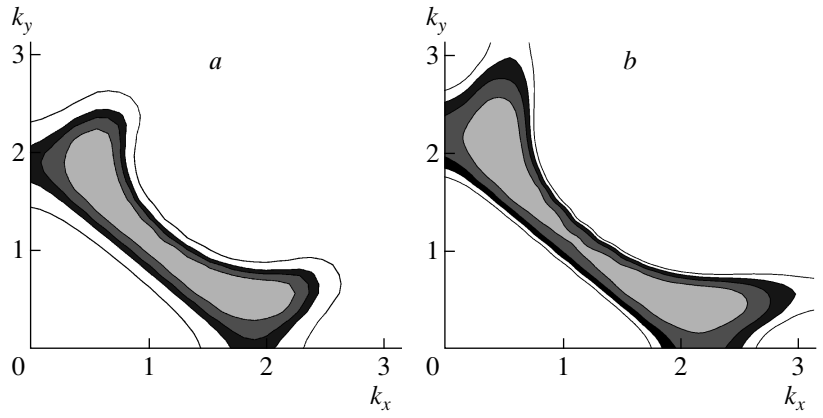

Fig. 16. $A(\mathbf{k}, \omega = 0)$ on the FS at $\delta = 0.05$ (a) and $\delta = 0.1$ (b) at $T = 0.03t$ for $\Delta = 4t$

self-energy in the classical limit in our approach and in the two-particle self-consistent approach (TPSC) [27] or in the model of short-range static spin (charge) fluctuations [15] are similar. Numerical results for the spectral density and the FS in the NCA approximation for the self-energy are quite similar to those obtained within the generalized DMFT [13, 15], where all diagrams for the electron scattering by spin (or charge) fluctuations in the static approximation were taken into account. Our results also agree with calculations based on the cluster approximation [12] and the TPSC [27].

In the present paper, we have not presented a fully self-consistent theory for the single-electron GF and the dynamical spin and charge susceptibility. This requires rather involved calculations of the collective spin and charge excitation spectra, which are beyond the scope of the present paper. Instead, we used a model for the dynamical spin susceptibility (26) that is usually employed in phenomenological approach. However, a variation of the electron (hole) interaction with spin fluctuations in our theory is strongly restricted because the interaction vertex is given by hopping parameters (2) in the Hubbard model, while the intensity of spin fluctuations at the AF wave-vector $\mathbf{Q}$ ($C(\xi)$ in the Table) determined by the AF correlation length ξ is fixed by the sum rule in (27). A variation of the cut-off energy ω_s does not noticeably affect the numerical results, as we have checked. The resulting coupling constant λ obtained in our calculations (see Sec. 3.4) seems to be too large compared with the ARPES results. This discrepancy can be caused by disregarding the scattering on charge fluctuations in the dynamical susceptibility model (25) and the electron–phonon interaction, which may reduce the contribution from the electron–spin interaction.

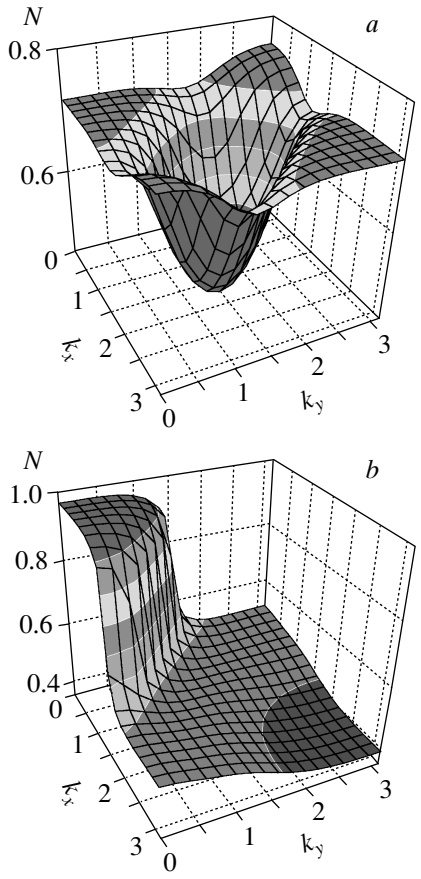

Fig. 17. The electronic occupation numbers $N_{\mathbf{k}}$ at $T = 0.03t$ for $\delta = 0.05$ (a) and at $\delta = 0.3$ (b) for $\Delta = 4t$

The main conclusion of the present study is that a decisive role in renormalization of the electron spectrum in a strongly correlated system such as cuprate

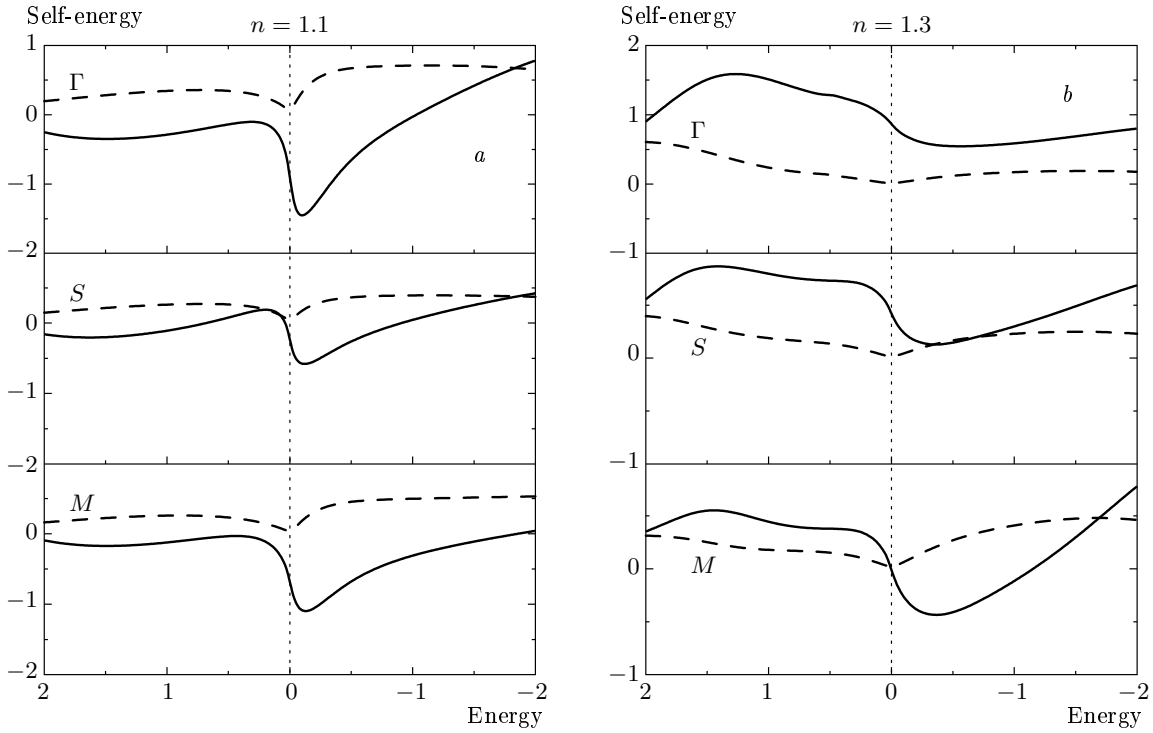

Fig. 18. Energy dependence of the real and imaginary parts of the self-energy $\Sigma(\mathbf{k}, \omega)$ for $\Delta = 4t$ at the $\Gamma(0,0)$, $S(\pi/2, \pi/2)$ and $M(\pi, \pi)$ points at $\delta = 0.1$ (a) and $\delta = 0.3$ (b)

superconductors is played by the electron interaction with spin fluctuations, which is in accord with other studies (see, e.g., [3, 12, 15]). The numerical results for the electron dispersion in Sec. 3.2, for the FS and the occupation numbers in Sec. 3.3, and for the self-energy in Sec. 3.4 unambiguously confirm this conclusion. As the doping or temperature increase, spin correlations are suppressed, which results in transition from a strong to a weak correlation limit. These observations were also confirmed by a consideration of the model with intermediate Coulomb correlations in Sec. 3.5. A theory of superconducting transition within the present theory will be considered elsewhere.

One of the authors (N. P.) is grateful to Prof. P. Fulde for the hospitality extended to him during his stay at MPIPKS, Dresden, where a major part of the present work was done.

REFERENCES

1. A. Damascelli, Z. Hussain, and Z.-X. Shen, Rev. Mod. Phys. **75**, 473 (2003).

2. M. V. Sadovskii, Usp. Phys. Nauk **171**, 539 (2001) [Physics–Uspekhi **44**, 515 (2001)].

3. M. Eschrig, Advances in Physics **55**, 47 (2006).

4. P. W. Anderson, Science **235**, 1196 (1987); P. W. Anderson, *The Theory of Superconductivity in the High-T_c Cuprates*, Princeton Univ. Press, Princeton (1997).

5. J. Hubbard, Proc. Roy. Soc. A **276**, 238 (1963); A **284**, 401 (1964).

6. N. Bulut, Adv. Phys. **51**, 1587 (2002).

7. G. Ovchinnikov and V. V. Valkov, *Hubbard Operators in the Theory of Strongly Correlated Electrons*, Imperial College Press, London (2004).

8. F. Mancini and A. Avella, Adv. Phys. **53**, 537 (2004).

9. A. Georges, G. Kotliar, W. Krauth, and M. Rozenberg, Rev. Mod. Phys. **68**, 13 (1996).

10. G. Kotliar, S. Y. Savrasov, K. Haule, V. S. Oudovenko, O. Parcollet, and C. A. Marianetti, Rev. Mod. Phys. **78**, 865 (2006).

11. Th. Maier, M. Jarrel, Th. Pruschke, and M. H. Hettler, Rev. Mod. Phys. **77**, 1027 (2005).

12. A.-M. S. Tremblay, B. Kyung, and D. Sénéchal, Fizika Nizkikh Temperatur (J. Low Temp. Phys.) **32**, 561 (2006).

13. M. V. Sadovskii, I. A. Nekrasov, E. Z. Kuchinskii, Th. Pruschke, and V. I. Anisimov, Phys. Rev. B **72**, 155105 (2005).

14. E. Z. Kuchinskii, I. A. Nekrasov, and M. V. Sadovskii, Pis'ma v Zh. Exp. Teor. Fiz. **82**, 217 (2005) [JETP Letters **82**, 198 (2005)].

15. E. Z. Kuchinskii, I. A. Nekrasov, and M. V. Sadovskii, Fizika Nizkikh Temperatur (J. Low Temp. Phys.) **32**, 528 (2006).

16. S. Krivenko, A. Avella, F. Mancini, and N. Plakida, Physica B **359–361**, 666 (2005).

17. Y. Kakehashi and P. Fulde, Phys. Rev. B **70**, 195102 (2004); J. Phys. Soc. Jpn. **74**, 2397 (2005).

18. D. N. Zubarev, Usp. Fiz. Nauk, **71**, 71 (1960) [Sov. Phys. Uspekhi **3**, 320 (1960)].

19. N. M. Plakida, R. Hayn, and J.-L. Richard, Phys. Rev. B **51**, 16599 (1995).

20. N. M. Plakida and V. S. Oudovenko, Phys. Rev. B **59**, 11949 (1999).

21. N. M. Plakida, L. Anton, S. Adam, and Gh. Adam, Zh. Exp. Theor. Fyz. **124**, 367 (2003) [JETP **97**, 331 (2003)].

22. L. F. Feiner, J. H. Jefferson, and R. Raimondi, Phys. Rev. B **53**, 8751 (1996).

23. V. Yu. Yushankhai, V. S. Oudovenko, and R. Hayn, Phys. Rev. B **55**, 15562 (1997).

24. V. J. Emery, Phys. Rev. Lett. **58**, 2794 (1987); C. M. Varma, S. Schmitt-Rink, and E. Abrahams, Sol. St. Comm. **62**, 681 (1987).

25. J. Jaklič and P. Prelovšek, Phys. Rev. Lett. **74**, 3411 (1995); **75**, 1340 (1995).

26. J. Bonca, P. Prelovšek, and I. Sega, Europhys. Lett. **10**, 87 (1989).

27. Y. Vilk and A.-M. Tremblay, J. Phys. Chem. Solids (UK) **56**, 1769 (1995).

28. T. Yoshida, X. J. Zhou, M. Nakamura et al., Phys. Rev. B **63**, 220501 (2001).

29. A. A. Kordyuk, S. V. Borisenko, A. Koitzsch, J. Fink, M. Knupfer, and H. Berger, Phys. Rev. B **71**, 214513 (2005).

30. M. M. Korshunov, V. A. Gavrichkov, S. G. Ovchinnikov, I. A. Nekrasov, Z. V. Pchelkina, and V. I. Anisimov, Phys. Rev. B **72**, 165104 (2005).

31. D. Sénéchal and A.-M. S. Tremblay, Phys. Rev. Lett. **92**, 126401 (2004).

32. Z. Liu and E. Manousakis, Phys. Rev. B **45**, 2425 (1992).